



Effects of Yb³⁺ Doping on Structural, Morphological, and Temperature Dependent Magnetic Properties of MnFe₂O₄ Nanoparticles

Sudha Gulati¹ · Shubha Gokhale² · Vandna Luthra³

Received: 27 January 2023 / Accepted: 27 February 2023 / Published online: 21 March 2023
© The Author(s), under exclusive licence to Springer Science+Business Media, LLC, part of Springer Nature 2023

Abstract

MnFe_{2-x}Yb_xO₄ nanoparticles ($x = 0, 0.025, 0.075, 0.1, 0.15, \text{ and } 0.2$) are synthesized using the co-precipitation method. The influence of rare earth Yb³⁺ doping on the manganese ferrite is investigated by techniques such as x-ray diffraction (XRD) and field effect scanning electron microscopy (FESEM). The magnetic properties were measured using vibrating sample magnetometer (VSM) at temperatures of 5 K and 300 K. XRD results show the formation of undoped and Yb³⁺-doped manganese ferrite nanoparticles. Crystallite size calculated using XRD reveals that it is doping concentration dependent. FESEM images reveal the formation of faceted nanoparticles for undoped sample and spherical shape for $x = 0.025\text{--}0.2$. Energy-dispersive X-ray spectroscopy (EDS) shows that Yb³⁺ ions are successfully incorporated into manganese ferrite. Saturation magnetization, coercivity, retentivity, squareness ratio, thickness of the dead layer, magnetic moment, and anisotropy constant are determined at 5 K and 300 K. These studies show dependence of these parameters on the amount of doping.

Keywords MnFe₂O₄ · Rare earth doped ferrites · Yb doping · Low temperature magnetic behaviour

1 Introduction

Spinel ferrites (MnFe₂O₄, CoFe₂O₄, NiFe₂O₄, etc.) have drawn the attention of numerous researchers due to their distinctive structural, electrical, and magnetic properties and they find use in a variety of uses like medical diagnosis, magnetic resonance imaging, antibacterial activities, targeted drug delivery, microwave devices, transformer cores, gas sensors, and storage devices [1–6]. Due to its special characteristics like high coercive field, low eddy losses, high saturation magnetization (M_s), high resistivity, etc., MnFe₂O₄ is being explored for suitability in these applications [7–9]. Spinel ferrites are cubic structures with the general formula AB₂O₄, where A represents a divalent transition metal cation like Zn, Mn, Cu, Co, or Ni, while B represents a trivalent cation such as Fe. They occupy the tetrahedral (A)

and octahedral (B) positions, respectively. Each unit cell of spinel ferrite comprises 56 atoms. The ion balance and site preference energy determine how the cations are distributed over these sites [10].

It is known that the substitution of rare earth (RE) in MnFe₂O₄ manifests into modification of its properties [11, 12]. The numbers of unpaired 4f electrons of RE ions are reported to affect the microstructure and various properties of substituted ferrites. In addition, the substitution with larger radii RE ions can further affect the properties of spinel ferrites. RE ions are reported to stabilize at octahedral sites, which culminates in causing internal stress and altering the cell symmetry. This causes the variation in structural, electrical, magnetic, and optical properties of spinel ferrites [13–15].

The properties of nanoparticles can be tailored by adjusting synthesis parameters like concentration of reactants, additives, pH value of reactants in the reaction vessel, stirring speed, duration of synthesis, annealing temperature, etc. [15, 16]. In the present work, co-precipitation method is used to synthesize the undoped and Yb-doped manganese ferrites. This method is simple, cost-effective, requires a low temperature, and produces material with high purity and yield [16].

The rare earth ytterbium (atomic number – 70 and atomic mass – 173.04 gmol⁻¹) is being used as a non-hazardous

✉ Sudha Gulati
sudhagulati@kalindi.du.ac.in

¹ Department of Physics, Kalindi College, East Patel Nagar, New Delhi 110008, India

² School of Sciences, Indira Gandhi National Open University, Maidan Garhi, New Delhi 110068, India

³ Department of Physics, Gargi College, Siri Fort Road, New Delhi 110049, India

and non-polluting catalyst. In a recent work by Ugender et al. on the temperature dependence of magnetic properties of $\text{NiFe}_{2-x}\text{Yb}_x\text{O}_4$ ($x=0, 0.05, 0.075$), it was shown that the magnetization and anisotropy constant decreased with increasing temperature [17]. However, it has been noted that when doping increases, the magnetization decreases and the anisotropy constant rises. Another study on bismuth ferrite at room temperature was carried out by Remya et al. [18]. In this study, an increase in dielectric constant and coercivity accompanied with a decrease in the dielectric loss, and M_S was observed with Yb doping ($x=0, 0.1, 0.2$).

Bulai et al. studied the structural, magnetic, and magnetostrictive properties of undoped and many rare earth dopants including Yb-doped cobalt ferrites [19]. The magnetostriction coefficient and strain derivative of the Yb-doped samples prepared by solid-state route were found to be the maximum which makes them suitable for sensing applications.

Raheem et al. synthesized the nanoparticles by microemulsion technique and examined the influence of Yb on the properties of $\text{Sr}_2\text{NiCoYbFe}_{28}\text{O}_{46}$ hexa-ferrites. They observed a decrease in M_S and coercivity was reported to be in the range 577–671 Oe with Yb doping from $x=0$ –0.15. [20]. Bibi et al. studied the electric and dielectric properties of ytterbium substituted magnesium ferrite materials $\text{MgYbFe}_{2-x}\text{O}_4$ [21]. Their studies showed a decrease in dielectric constant with an increase in frequency. They also observed a decrease in M_S and an increase in coercivity as well as a decrease in crystallite size with an increase in Yb doping. Alonzian et al. reported ytterbium-doped manganese ferrite's structural and magnetic properties. These studies indicated a decrease in M_S and an increase in coercivity with a decrease in crystallite size [22]. In all of the above studies, coercivity was reported to be higher than 100 Oe.

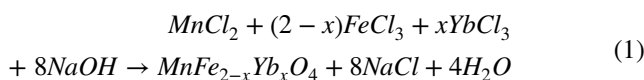
Manganese ferrite is more biocompatible than other ferrites, which makes it better suited for biomedical applications which includes magnetic resonance imaging (MRI) [10, 23]. This work aims to provide a detailed investigation of the effect of Yb doping of MnFe_2O_4 on the structural, morphological, and magnetic properties which could be helpful in exploring their use for various applications.

2 Experimental

2.1 Synthesis

The undoped and Yb-doped manganese ferrite nanoparticles were synthesized using the co-precipitation method. In this synthesis process, the stoichiometric amount of $\text{MnCl}_2 \cdot 4\text{H}_2\text{O}$ was mixed in de-ionized (DI) water to form a 1.0 M solution and the measured quantities of FeCl_3 along with $\text{YbCl}_3 \cdot \text{H}_2\text{O}$ were mixed in DI water to form a 2.0 M solution. Both the

solutions were ultrasonicated at room temperature for 5 min, mixed and then the resultant solution (solution 1) was heated up to 60 °C while continuously stirring on a magnetic stirrer. The solution of NaOH with 1.3 molarity was prepared in deionized water (solution 2). This was boiled and then added to solution 1. The mixture was maintained at 85 °C for 2 h under magnetic stirring. The resultant precipitate of synthesized nanoparticles was washed thoroughly in DI water several times followed by an ethanol wash. Vacuum-drying was used to dry the sample, which was then ground using a mortar and pestle to obtain the black-coloured powder of $\text{MnFe}_{2-x}\text{Yb}_x\text{O}_4$. This procedure was repeated to obtain $\text{MnFe}_{2-x}\text{Yb}_x\text{O}_4$ nanoparticles for various values of $x=0, 0.025, 0.075, 0.1, 0.15, \text{ and } 0.2$. The chemical reaction for the formation of $\text{MnFe}_{2-x}\text{Yb}_x\text{O}_4$ can be represented as follows:



2.2 Characterizations

The X-ray diffraction (XRD) patterns were recorded on a Bruker, D8 Discover High-Resolution X-ray Diffractometer using CuK_α radiation ($\lambda=1.5406 \text{ \AA}$) at 45 kV and 40 mA and was used to investigate the crystal structure, as well as phase purity of all the samples. XRD patterns were recorded for 2θ values from 10 to 80°. The crystallite size (cs) and phase of various samples were determined using the XRD data. The surface morphology, crystallite size, and microstructure of the samples were studied using Zeiss Gemini SEM500 equipped with energy-dispersive x-ray spectroscopy (EDS). The magnetic properties were inferred from the hysteresis loop obtained using a Cryogenic Limited manufactured Physical Properties Measurement System (PPMS) with the magnetic field varying from $-10,000$ to $10,000$ Oe at 300 K and 5 K. The values of saturation magnetization (M_S), coercivity (H_C), and remnant magnetization (M_r) were obtained. Furthermore, other parameters like squareness ratio ($S = M_r/M_S$), magnetic moment (μ), and anisotropy constant (K_a) were estimated.

3 Results and Discussions

3.1 XRD Studies

Crystallite size is calculated from the XRD data using the Debye–Scherrer formula [24]:

$$cs = \frac{0.9\lambda}{\beta \cos \theta} \quad (2)$$

where λ ($= 1.5406 \text{ \AA}$) is the wavelength of x-ray, β is the full width at half maximum of the main diffraction peak expressed in radian, and θ is the Bragg angle of the strongest peak.

The lattice constant a was calculated for different samples using the Eq. (3) applied at the strongest peak (311). Here, (hkl) represents the Miller indices [24]:

$$a = \frac{\lambda \sqrt{h^2 + k^2 + l^2}}{2 \sin \theta} \quad (3)$$

The XRD patterns of the prepared $\text{MnYb}_x\text{Fe}_{2-x}\text{O}_4$ (where $x = 0, 0.025, 0.075, 0.1, 0.15, 0.2$) measured at 300 K are shown in Fig. 1.

XRD peaks were observed to be at $29.9^\circ, 35.1^\circ, 42.7^\circ, 56.3^\circ$, and 61.8° for the undoped sample. The peaks are indexed as (220), (311), (400), (422), (333), and (440). The peaks match well with the data from JCPDS card no. 74–2403 for cubic MnFe_2O_4 having $Fd\text{-}3m$ space group [7, 9, 12]. There are no peaks due to any other impurity or secondary phases. The lack of such extra phases in the current study demonstrates that the Yb^{3+} ions are soluble in the host material and validates the effectiveness of the synthesis method in incorporating Yb ions into the manganese ferrite matrix in spite of wide difference in the ionic radii. Good crystallinity of the samples can be concluded from the sharp and XRD peaks. The peak shifting was observed in all the XRD patterns of the doped samples. These shifts in peak position indicate the incorporation of Yb^{3+} ions into MnFe_2O_4 in the samples. The variation of crystallite size (cs) with Yb doping is shown in Fig. 2a.

In the present work, crystallite size is observed in the range of 24.8–34.7 nm. Though the ionic radius of the Yb^{3+} ion (0.86 \AA) is more than the ionic radius of the Fe^{3+} ion (0.63 \AA), it is observed that the incorporation of Yb^{3+} ions results into crystallite size (cs) in the range of 24.8–28.9 nm, which is smaller than cs of the undoped sample, for lower values of dopant concentration x ($x \leq 0.1$). Such variations were also observed in the literature [18, 19, 25]. As Yb^{3+}

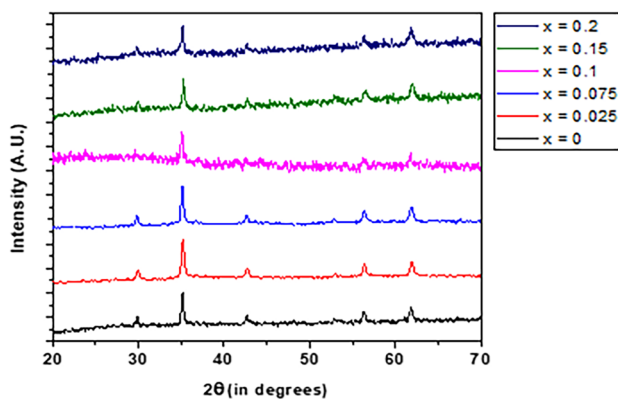


Fig. 1 X-ray diffraction (XRD) pattern of $\text{MnYb}_x\text{Fe}_{2-x}\text{O}_4$ nanoparticles (where $x = 0, 0.025, 0.075, 0.1, 0.15, 0.2$)

doping is initiated ($x = 0.025$), it may give rise to a large number of seeds for crystal growth and lead to more number of smaller crystallites forming in the solution. Further increase in the amount of doping of Yb^{3+} leads to an increase in cs which may be due to the incorporation of a larger radii dopant Yb^{3+} as compared to Fe^{3+} . Such variations in cs with doping x have also been reported in the literature.

The incorporation of Yb^{3+} into the spinel crystal structure has its significant effect also on lattice constant as is evident in Fig. 2b.

Both decrease and increase in lattice constant with doping were observed. The incorporation of Yb^{3+} in the spinel structure may cause iron vacancies, distortion in tetrahedral and octahedral symmetry, and has an impact on the lattice parameter and bond length. Hence, it makes sense that ferrites with Yb^{3+} doping have a drop in lattice parameter. However, a rise in the lattice parameter is also seen, which is a result of the large size Yb^{3+} ions replacing the smaller transition metal ions. Such variations have been reported in the literature [26–28]. In the present work, the lattice parameter of undoped MnFe_2O_4 is calculated to be 8.455 \AA and lattice parameters for the doped samples were in the range $8.423\text{--}8.469 \text{ \AA}$.

3.2 FESEM Analysis

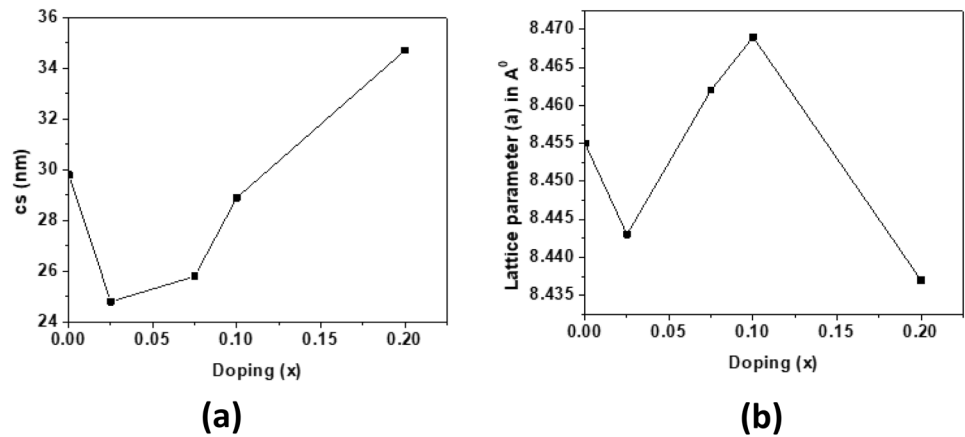
Figure 3 shows the FESEM images for all the samples from which the morphology of synthesized nanoparticles can be investigated.

Figure 3a indicates that most of the particles of undoped MnFe_2O_4 have a faceted shape. Figure 3b–e show spherical-shaped nanoparticles with agglomeration. As Yb^{3+} substitutes for the lighter and smaller Fe^{3+} ions, it introduces strain in the lattice which leads to isotropic growth as is evident in the FESEM images [29].

In Fig. 4, EDS spectra of representative samples ($x = 0$ and 0.1) are shown. The detailed data for all the samples is given in Table 2. The characteristic x-ray peaks of Mn, Fe, Yb, and O atoms evident in EDS of $\text{MnFe}_{2-x}\text{Yb}_x\text{O}_4$ are shown in Fig. 4. It shows the peaks of Fe, Mn, O, and Yb elements and does not show peaks corresponding to any other element which established the purity of the samples. Table 1 shows the weight and atomic percentages of elements O, Mn, Fe, and Yb in $\text{MnFe}_{2-x}\text{Yb}_x\text{O}_4$ ($x = 0, 0.025, 0.075, 0.1, \text{ and } 0.2$) obtained from EDS analysis.

The obtained percentages and the initial stoichiometric ratios in these samples may vary due to a number of instrument and process software settings like the data acquisition time, dead time, work distance, and acceleration voltage. However, the atomic ratios of Mn/Fe or Mn/(Fe + Yb) are nearly 0.5. The relative percentages of Yb/Fe may vary from expected values arising due to the mismatch between the ionic radii of Fe and Yb ions. However, an increase in the

Fig. 2 **a** Crystallite size (*cs*) and **b** lattice parameter of undoped and Yb-doped samples



percentage of Yb with an increase in *x* is clearly evident confirming systematically enhanced incorporation of Yb in manganese ferrite.

3.3 Magnetic Studies

Magnetic characterization of $\text{MnFe}_{2-x}\text{Yb}_x\text{O}_4$ nanoparticles was carried out using VSM and magnetization curves as shown in Fig. 5 at temperatures of 300 K and 5 K with the insets showing the magnified plots highlighting the variation in the coercivity with temperature.

The magnetic moment (μ) per formula unit is calculated by Eq. (4) [30]:

$$\mu = \frac{M_S * M}{\mu_B * N_A} \quad (4)$$

where M_S , M , μ_B , and N_A are the saturation magnetization, molecular weight, Bohr magneton, and Avogadro's number, respectively.

The magnetic anisotropy constant K_a is determined using the following relation [31]:

$$k_a = \frac{M_S * H_C}{0.96} \quad (5)$$

It has been reported that a magnetic dead layer is formed at the surface of the magnetic nanoparticle which can be attributed to the presence of highly anisotropic layer, surface

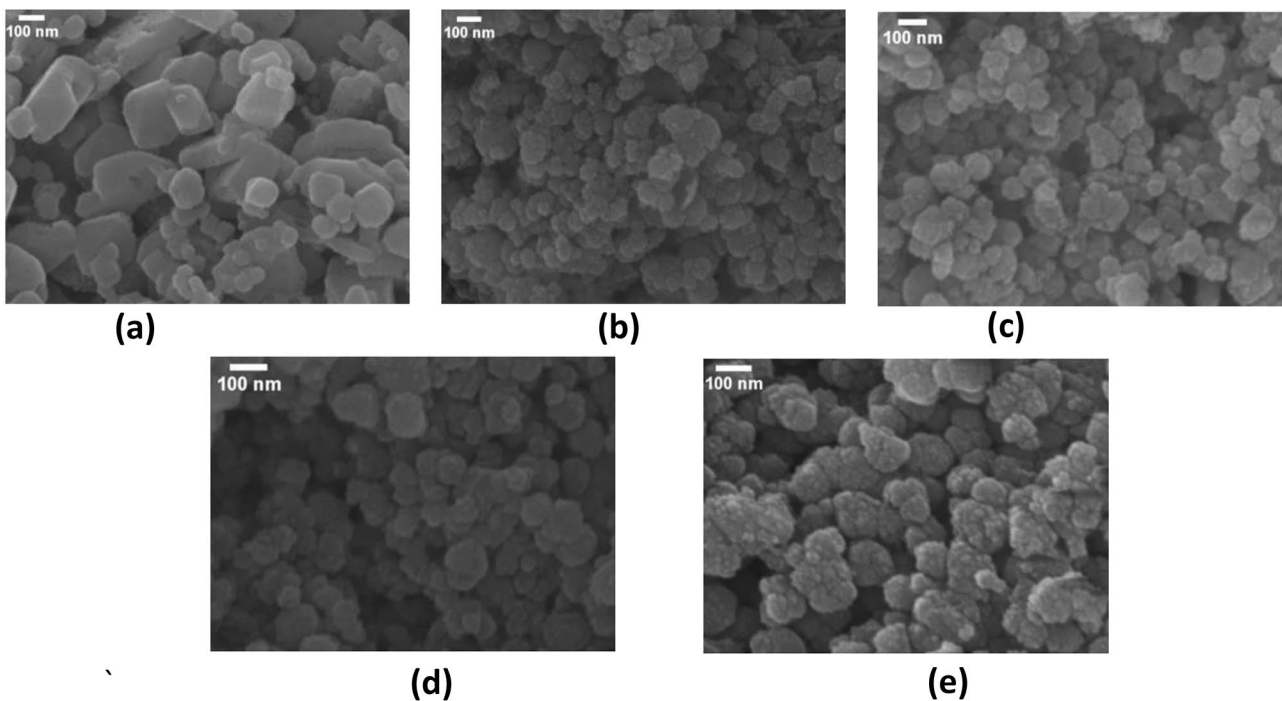


Fig. 3 FESEM images of $\text{MnYb}_x\text{Fe}_{2-x}\text{O}_4$ nanoparticles. **a** *x* = 0, **b** *x* = 0.025, **c** *x* = 0.075, **d** *x* = 0.1, and **e** *x* = 0.2

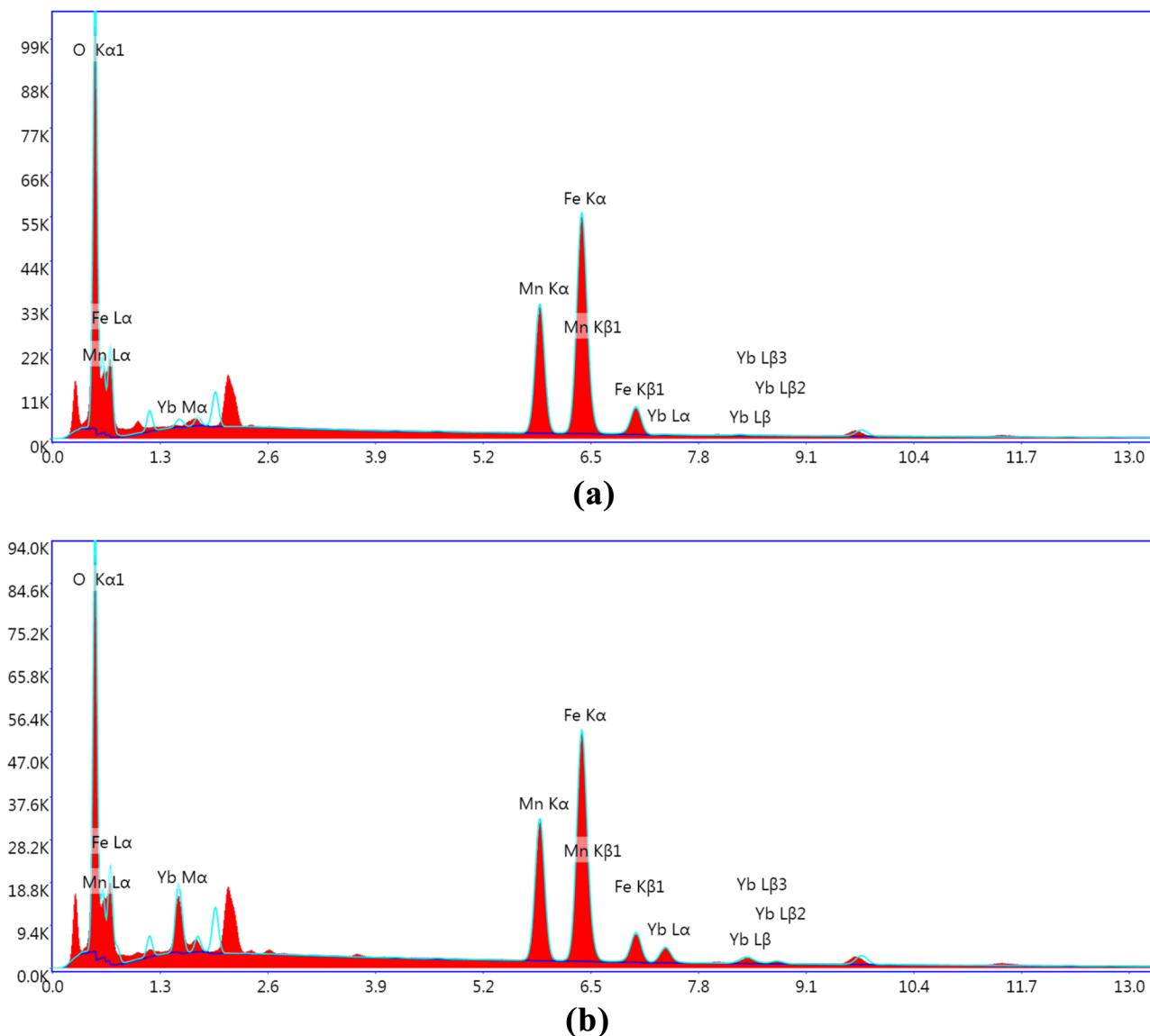


Fig. 4 EDS spectra of $MnYb_xFe_{2-x}O_4$ nanoparticles. **a** $x=0$ and **b** $x=0.2$

spin canting, or disruptions of the long-range order [32]. The saturation magnetization M_S of nanoparticles, that of the related bulk material M_{sb} , the thickness of the dead layer t , and the crystallite size cs are related by Eq. (6) [33, 34].

$$M_S = M_{sb} \left(1 - \frac{6t}{cs}\right) \tag{6}$$

The saturation magnetization (M_S), coercivity (H_c), retentivity (Mr), the ratio t/cs , squareness ($S = M_r/M_S$),

Table 1 Weight % and atomic % of the elements O, Mn, Fe, and Yb in $MnYb_xFe_{2-x}O_4$ ($x=0, 0.025, 0.075, 0.1, \text{ and } 0.2$) obtained from EDS analysis

Element	$x=0$		$x=0.025$		$x=0.075$		$x=0.1$		$x=0.2$	
	Wt%	At %	Wt %	At %	Wt %	At %	Wt %	At%	Wt %	At%
O	25.40	54.24	25.26	54.40	14.29	37.40	17.18	43.00	23.22	53.34
Mn	24.76	15.40	24.23	15.20	28.02	21.36	27.04	19.71	23.37	15.63
Fe	49.51	30.29	48.69	30.04	53.74	40.29	50.22	36.01	44.19	29.07
Yb	-	-	1.81	0.36	3.94	0.95	5.55	1.28	9.22	1.96

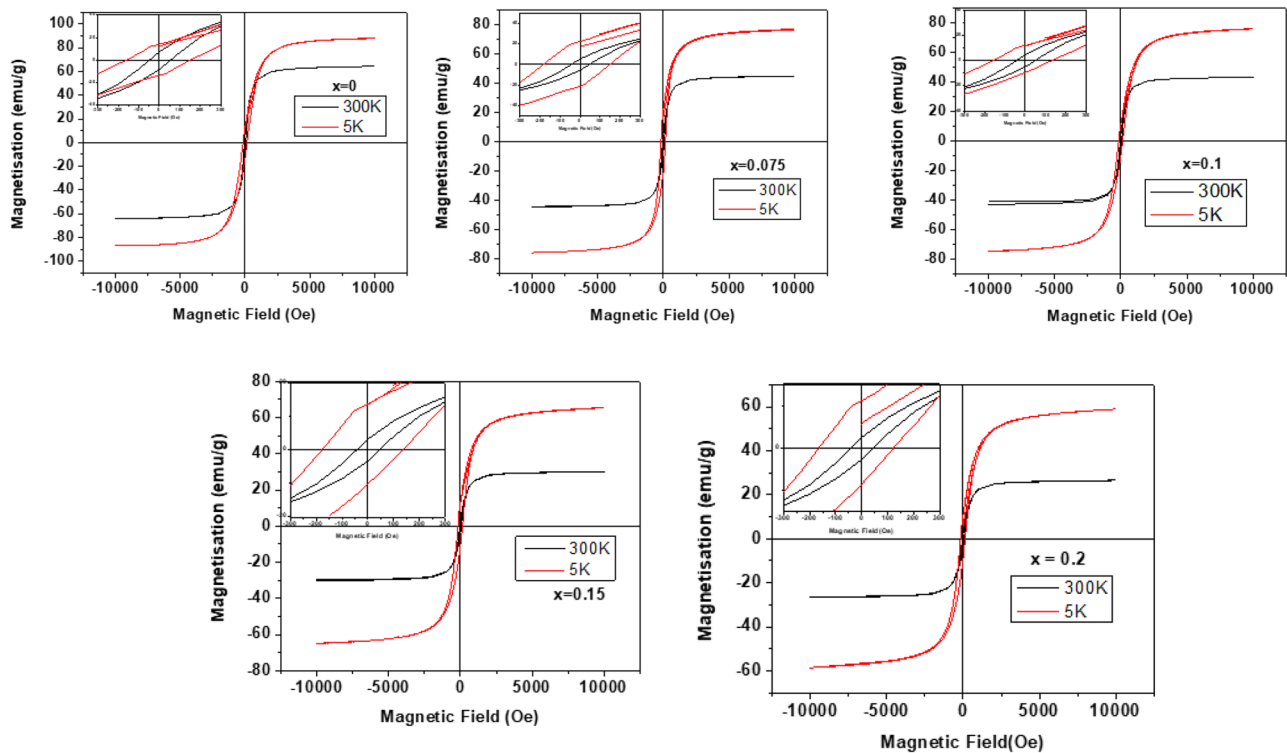


Fig. 5 Magnetisation curves of $\text{MnFe}_{2-x}\text{Yb}_x\text{O}_4$ ($x=0, 0.075, 0.1, 0.15,$ and 0.2) nanoparticles at 5 K and 300 K

magnetic moment (μ), and anisotropy constant (K_a) are recorded in Table 2.

The values of magnetic parameters in Table 2 are depicted in Fig. 6.

The magnetic moments of Fe^{3+} , Mn^{2+} , Fe^{2+} ions, and Yb^{3+} ions are $5 \mu_B$, $5 \mu_B$, and $4 \mu_B$, and $4.53 \mu_B$ (μ_B is Bohr magnetron),

respectively [17, 35]. When Yb^{3+} ions of bigger size with magnetic moment $4.53 \mu_B$ replaces Fe^{3+} ions of smaller size with magnetic moment $5 \mu_B$, then magnetic properties vary from the properties of the undoped MnFe_2O_4 .

Figure 6 depicted the variation of M_S , H_C , and M_r at temperatures 300 K and 5 K. The magnetic behaviour of

Table 2 Saturation magnetization (M_S), coercivity (H_C), retentivity (M_r), squareness (S), magnetic moment (μ), and anisotropy constant (K_a) of $\text{MnFe}_{2-x}\text{Yb}_x\text{O}_4$ samples at 300 K and at 5 K

At room temperature 300 K							
x	$M_S(\text{emu/g})$	$H_C(\text{Oe})$	$M_r(\text{emu/g})$	t/cs	$S = M_r/M_S$	$\mu(\mu_B)$	$K_a(\text{emug}^{-1}\text{Oe})$
0.00	64.4	52.00	7.84	0.03	0.12	2.66	3417
0.025	53.5	48.81	6.05	0.05	0.11	2.24	2720
0.075	44.7	45.09	5.27	0.07	0.12	1.92	2057
0.10	43.0	45.95	4.75	0.08	0.11	1.87	2016
0.15	30.1	44.86	3.25	0.10	0.11	1.34	1376
0.2	26.5	43.00	2.59	0.11	0.09	1.21	1163
At temperature 5 K							
x	$M_S(\text{emu/g})$	$H_C(\text{Oe})$	$M_r(\text{emu/g})$	t/cs	M_r/M_S	$\mu(\mu_B)$	$K_a(\text{emug}^{-1}\text{Oe})$
0	88.1	154.0	13.75	0.16	0.16	3.64	14133
0.075	76.2	167.0	22.00	0.29	0.23	3.27	13255
0.1	75.5	145.3	10.50	0.14	0.29	3.28	11207
0.15	65.5	155.5	12.00	0.18	0.14	2.91	9825
0.2	58.3	144.0	10.06	0.17	0.18	2.65	8532

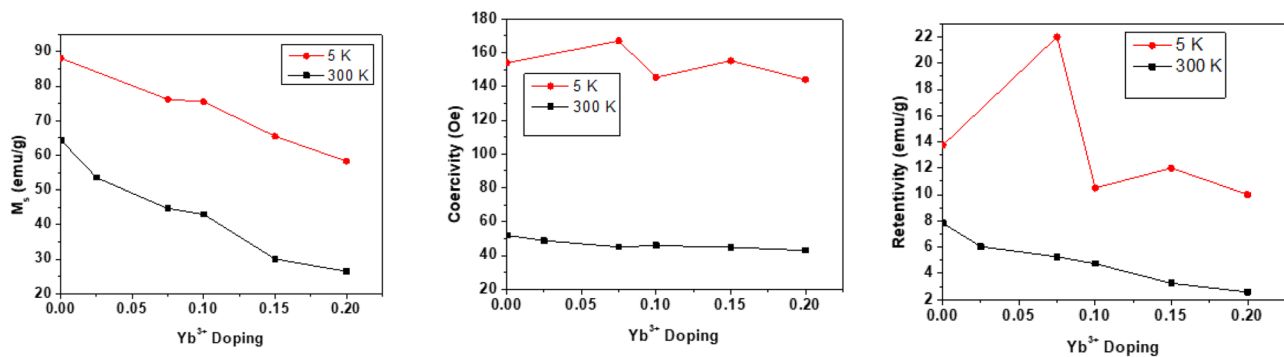


Fig. 6 Variation of saturation magnetisation, coercivity, and retentivity of $\text{MnFe}_{2-x}\text{Yb}_x\text{O}_4$ nanoparticles at 300 K and 5 K

Yb^{3+} -doped manganese ferrite can be attributed to various reasons such as rearrangement of the cations, crystallite size, deficiency of oxygen anions, exchange interactions between cations, and ionic radius of dopant. The incorporation of Yb^{3+} ions in manganese ferrite creates two new types of interactions in addition to Fe^{3+} - Fe^{3+} interaction. These are Yb^{3+} - Fe^{3+} interactions and Yb^{3+} - Yb^{3+} interactions. Both these interactions are weaker as compared to Fe^{3+} - Fe^{3+} interaction culminating in a decrease in M_S at temperatures 300 K and 5 K with increase in x [36, 37]. Table 2 shows the calculated values of t/cs for all these samples and further supports the fact that M_S decreases with the increase of the ratio t/cs . This can be attributed to the increased effects of an inactive magnetic layer on the surface of nanoparticles with an increase in dopant concentration x .

It is evident from Fig. 6 that M_S increased as temperature was decreased from 300 to 5 K. This increase in M_S can be attributed to a decrease in thermal energy, and thereby lowering the thermal fluctuations in magnetic moment. At low temperatures, “surface spin freezing” effect is reported to be manifested in case of MnFe_2O_4 nanoparticles [38].

Figure 6 also indicates that the coercivity values (H_C) decrease with Yb^{3+} doping in manganese ferrite at 300 K. The value of room temperature H_C ranges between 52 and 30.1 Oe in $\text{MnFe}_{2-x}\text{Yb}_x\text{O}_4$ (for $x=0$ to 0.15). These results match well with the reported literature [39]. The coercivity is known to be controlled by various factors like grain size, magnetic particle shape, stresses, and different exchange couplings present in the core and at the surface. Such materials are being used for hyperthermia treatment [40].

The critical diameter for a MnFe_2O_4 particle at $T=300$ K was determined to be 42.9 nm by Rafique et al., below which the particle exhibits superparamagnetism [41]. The particle size limit for MnFe_2O_4 particles is 42 nm, according to Gnanaprakash et al. [42]. The crystallite size of synthesized MnFe_2O_4 particles ~ 24.8 – 34.7 nm, which is smaller than the calculated critical size limit demonstrating the samples’ superparamagnetic properties. However, finite coercivity

(~ 43 – 52 Oe) values indicate near superparamagnetic nature of these nanoparticles.

As the temperature is lowered from 300 to 5 K, coercivity H_C is found increase from 52 to 152 Oe for undoped MnFe_2O_4 . The same trend for H_C is also observed for all the doped $\text{MnFe}_{2-x}\text{Yb}_x\text{O}_4$ nanoparticles. Table 3 indicates that coercivity H_C has higher values in the range of 167–140 Oe at 5 K for all the doped samples. At lower temperatures, the surface spins of synthesized nanoparticles freeze in random states and are cannot align along the field direction resulting into increased the coercivity. The coercivity is 167 Oe for the sample $x=0.075$ at 5 K which is the highest among all the samples. A rise in coercivity at low temperature enhances hysteresis loss and hence, the nanoparticles can be explored to make a permanent magnet.

It can be noted from Table 2 that the magnetic moment μ , which is proportional to the M_S , decreases with increase in dopant concentration x at 300 K and 5 K. In the present work, both M_S and μ have the largest value for the undoped sample at 300 K and 5 K. These values decrease with an increase in doping. A rise or fall in magnetic moment value indicates the enhancement or reduction of the superexchange interactions [30].

As revealed from the data in Table 2, the magnetic anisotropy constant K_a reduces with the increase in doping both at 300 K and 5 K. The lowering of anisotropy constant with doping can be attributed to lower concentration of Mn^{2+} ions at the octahedral site [43].

However, K_a is higher for all the samples at a 5 K as compared to at 300 K. This is can be directly correlated to the enhanced values of saturation magnetization and coercivity at lower temperature.

According to the Stoner–Wohlfarth (S–W) theory, the squareness S has two possible values: ~ 0.83 and ~ 0.5 related to cubic and uniaxial anisotropies, respectively [30, 31]. Table 2 shows that S has values ~ 0.1 (i.e. < 0.5), which may be due to surface spin disorder effects. The smaller value of the squareness S (less than 0.5) suggests a multi-domain

structure with uniaxial anisotropy and incomplete coupling in these samples [28]. An increase in the squareness ratio as compared to 300 K has been observed at 5 K; however, it is also lower than 0.5.

4 Conclusions

In the present work, $\text{MnFe}_{2-x}\text{Yb}_x\text{O}_4$ nanoparticles ($x=0\text{--}0.2$) are prepared using the co-precipitation method. The effect of rare earth Yb^{3+} doping on the structural and magnetic properties is studied by various techniques like x-ray diffraction (XRD), field effect scanning electron microscopy (FESEM), and vibrating sample magnetometer at 5 K and 300 K. The crystallite sizes estimated are in the range of 24–35 nm. Crystallite size at 300 K depend on the amount of dopant Yb^{3+} . Different magnetic properties obtained at 300 K and 5 K show the dependence on the amount of doping and temperature. The values of calculated squareness are in the range of 0.09–0.29 suggesting a multi-domain structure with uniaxial anisotropy and incomplete coupling. As the doping is increased, the saturation magnetization and coercivity decrease; however, at lower temperatures, coercivity and saturation magnetization both increase. These nanoparticles can be explored to make a permanent magnet at low temperature.

Acknowledgements The experimental work for the synthesis of nanoparticles was carried out in the Physics Laboratory, School of Sciences, Indira Gandhi National Open University, Maidan Garhi, New Delhi 110068. The authors would like to thank “University Science Instrumentation centre (USIC), Department of Physics, University of Delhi, Delhi” for the XRD measurements and FESEM. The authors acknowledge the Advanced Instrumentation Research Facility (AIRF), Jawaharlal Nehru University (JNU), Delhi for VSM measurements.

Declarations

Conflict of Interest The authors declare no competing interests.

References

- Manohar, A., Krishnamoorthi, C.: Synthesis and magnetic hyperthermia studies on high susceptible $\text{Fe}_{1-x}\text{Mg}_x\text{Fe}_2\text{O}_4$ superparamagnetic nanospheres. *J. Magn. Magn. Mater.* **443**, 267 (2017)
- Baykal, A., Kasapoğlu, N., Köseoğlu, Y.: Microwave-induced combustion synthesis and characterization of $\text{Ni}_x\text{Co}_{1-x}\text{Fe}_2\text{O}_4$. *Cent. Eur. J. Chem.* **6**, 125 (2008)
- Ansari, M.M.N., Khan, S., Ahmad, N.: Effect of R^{3+} ($\text{R} = \text{Pr}, \text{Nd}, \text{Eu}$ and Gd) substitution on the structural, electrical, magnetic and optical properties of Mn-ferrite nanoparticles. *J. Magn. Magn. Mater.* (2018). <https://doi.org/10.1016/j.jmmm.2018.05.071>
- Gaffoor, A., Naidu, K.C.B., Ravinder, D., Batoor, K.M., Adil, S.F., Khan, M.: Synthesis of nano- $\text{Ni}_x\text{Fe}_2\text{O}_4$ ($X = \text{Mg}/\text{Co}$) by citrate-gel method: structural, morphological and low-temperature magnetic properties. *Appl. Phys. A*. **126**, 1:39 (2019)
- Rahman, K.R., Chowdhury, F.U.Z. and Khan, M.N.I.: Influence of Al^{3+} substitution on the electrical resistivity and dielectric behavior of $\text{Ni}_{0.25}\text{Cu}_{0.20}\text{Zn}_{0.55}\text{Al}_x\text{Fe}_{2-x}\text{O}_4$ ferrites synthesized by solid state reaction technique. *J. Magn. Magn. Mater.* **443**, 366 (2017)
- Mornet, S., Vasseur, S., Grasset, F., Duguet, E.: Magnetic nanoparticle design for medical diagnosis and therapy. *J. Mater. Chem.* **14**(14), 2161 (2014)
- Ahalya, K., Suriyanarayanan, N., Ranjithkumar, V.: Effect of cobalt substitution on structural and magnetic properties and chromium adsorption of manganese ferrite nano particles. *J. Magn. Magn. Mater.* **372**, 208 (2014)
- Kumar, S., Shinde, T.J., Vasambekar, P.N.: Study of conduction phenomena in indium substituted Mn-Zn nanoferrites. *J. Magn. Magn. Mater.* **379**, 179 (2015)
- Vijaya, J.J., Sekaran, G., Bououdina, M.: Effect of Cu^{2+} doping on structural, morphological, optical and magnetic properties of MnFe_2O_4 particles/sheets/flakeslike nanostructures. *Ceram. Int.* **41**, 15 (2014)
- Asghar, K., Qasim, M., Da, D.: Preparation and characterization of mesoporous magnetic $\text{MnFe}_2\text{O}_4@ \text{mSiO}_2$ nanocomposite for drug delivery application. *Mater. Today. Proc.* **26**, 87 (2020)
- Salah, L.M., Moustafa, A.M., Farag, I.S.A.: Structural characteristics and electrical properties of copper doped manganese ferrite. *Ceram. Int.* **38**, 5605 (2012)
- Gopalan, E.V., Al-Omari, I.A., Malini, K.A., Joy, P.A., Kumar, D.S., Yoshida, Y., Anantharaman, M.R.: Impact of zinc substitution on the structural and magnetic properties of chemically derived nanosized manganese zinc mixed ferrites. *J. Magn. Magn. Mater.* **321**, 1092 (2009)
- Sattar, A.A.: Physical, magnetic and electrical properties of Ga substituted Mn-ferrites. *Egyptian J. Sol.* **27**, 99 (2004)
- Rezlescu, N., Rezlescu, E., Pasnicuand, C., Craus, M.: Effects of the rare-earth ions on some properties of a nickel-zinc ferrite. *J. Phys. Condens. Matter* **6**, 5707 (1994)
- Nagarajan, V., Thayumanavan, A.: Spray deposited MnFe_2O_4 thin films for detection of ethanol and acetone vapors. *Appl. Surf. Sci.* **428**, 748 (2018)
- Dippong, T.: Erika Andrea Levei and Oana Cadar; Recent advances in synthesis and applications of MFe_2O_4 ($\text{M} = \text{Co}, \text{Cu}, \text{Mn}, \text{Ni}, \text{Zn}$). *Nanoparticles Nanomaterials* **11**, 1560 (2021)
- Kodam, U., Raghavendra Reddy, V., Markandeyulu, G.: Temperature dependence of magnetization, anisotropy, and hyperfine fields of $\text{NiFe}_{2-x}\text{Yb}_x\text{O}_4$ ($x = 0, 0.05, 0.075$). *IEEE Transac. Magn.* **52**, (1) (2016). <https://doi.org/10.1109/INTMAG.2015.7157090>
- Remya, K.P., Amirthapandian, S., Manivel Raja, M., Viswanathan, C., Ponpandian, N.: Effect of Yb substitution on room temperature magnetic and dielectric properties of bismuth ferrite nanoparticles. *J. Appl. Phys.* **120**, 134304 (2016)
- Bulai, G., Diamandescu, L., Dumitru, I., Gurlui, S., Feder, M., Caltun, O.F.: Effect of rare earth substitution in cobalt ferrite bulk materials. *J. Magn. Magn. Mater.* **390**, 123 (2015)
- Raheem, F.: Muhammad Azhar Khan, Abdul Majeeda, Altaf Hussaina, Muhammad Farooq Warsi and Majid Niaz Akhtar; Structural, spectral, electrical, dielectric and magnetic properties of Yb doped SrNiCo-X hexagonal nano-structured ferrites. *J. Alloy. Compd.* **708C**, 903 (2017)
- Bibi, K., Ali, I., Farid, M.T., Mahmood, A., Ramay, S.M., Ali, K.: Electric and dielectric properties of ytterbium substituted spinel ferrites. *J. Mater. Sci. Mater. Electron.* **29**, 3744 (2018). <https://doi.org/10.1007/s10854-017-8308-1>
- Norah, H.: Alonizan and Rabia Qindeel; Structural and magnetic properties of ytterbium substituted spinel ferrites. *Appl. Phys. A* **124**, 408 (2018)
- Ugelstad, J., Berge, A., Ellingsen, T, et al.: Preparation and application of new monosized polymer particles. *Prog. Polym. Sci.* **17**, 87 (1992)
- Richa, J.: A review on the development of XRD in ferrite nanoparticles. *J. Supercond. Novel Magn.* <https://doi.org/10.1007/s10948-022-06213-9>
- Tatarchuk, T., Myslin, M., Mironyuk, I., Bououdina, M., Pędziwiatr, A.T., Gargula, R., Bogacz, B.F., Kurzydło,

- P.: Synthesis, morphology, crystallite size and adsorption properties of nanostructured Mg Zn ferrites with enhanced porous structure. *J. Alloys Comp.* **819**, 152945 (2020)
26. Zhao, B., Nan, Z.: One-pot synthesis of ZnLa xFe 2-x O4 clusters without any template and their possible application in water treatment. *J. Mater. Chem.* **22**, 6581–6586 (2012)
 27. Lohar, K.S., Pachpinde, A.M., Langade, M.M., Kadam, R.H., et al.: Self-propagating high temperature synthesis, structural morphology and magnetic interactions in rare earth Ho³⁺ doped CoFe₂O₄ nanoparticles. *J. Alloy. Compd.* **604**, 204–210 (2014)
 28. Gadkari, A.B., Shinde, T.J., Vasambekar, P.N.: Synthesis, characterization and magnetic properties of La³⁺ added Mg–Cd ferrites prepared by oxalate co-precipitation method. *J. Alloy. Compd.* **509**, 966–972 (2011)
 29. Jacob, B.P., Thankachan, S., Xavier, S., Mohammed, E.M.: Effect of Tb³⁺ substitution on structural, electrical and magnetic properties of sol–gel synthesized nanocrystalline nickel ferrite. *J. Alloys Comp.* **578**, 314 (2013)
 30. Almessiere, M.A., Slimani, Y., Gungunes, H., Manikandan, A., Baykal, A.: Investigation of the effects of Tm³⁺ on the structural, microstructural, optical, and magnetic properties of Sr hexaferrites. *Results in Physics* **13**, 102166 (2019)
 31. Almessiere, M.A., Slimani, Y., Sertkol, M., Nawaz, M., Sadaqat, A., Baykal, A., Ercan, I., Ozcelik, B.: Effect of Nb³⁺ substitution on the structural, magnetic, and optical properties of Co_{0.5}Ni_{0.5}Fe₂O₄ nanoparticles. *Nanomaterials.* **9**, 430 (2019)
 32. El-Sayed, H.M., Ali, I.A., Azzam, A., Sattar, A.A.: Influence of the magnetic dead layer thickness of Mg–Zn ferrites nanoparticle on their magnetic properties. *J Magn. Magn. Mater.* <https://doi.org/10.1016/j.jmmm.2016.10.049>
 33. He, X., Zhong, W., Au, C.T., et al.: Size dependence of the magnetic properties of Ni nanoparticles prepared by thermal decomposition method. *Nanoscale Res Lett* **8**, 446 (2013). <https://doi.org/10.1186/1556-276X-8-446>
 34. Tang, Z.X., Sorensen, C.M., Klabunde, K.J., Hadjipanayis, G.C.: Size-dependent Curie temperature in nanoscale MnFe₂O₄ particles. *Phys Rev Lett.* **67**, 3602 (1991)
 35. Jain, R., Luthra, V., Arora, M.: Shubha Gokhale; Infrared spectroscopic study of magnetic behavior of dysprosium doped magnetite nanoparticle. *J. Supercond. Novel Magn.* (2018). <https://doi.org/10.1007/s10948-018-4717-5s>
 36. Chen, Z., Du, Y., Li, Z., Yang, K., Lv, X.: Controllable synthesis of magnetic Fe₃O₄ particles with different morphology by one-step hydrothermal route. *J. Magn. Magn. Mater.* **426**, 121 (2017)
 37. Sabale, S.R.: Studies on catalytic activity of MnFe₂O₄ and CoFe₂O₄ MNPs as mediators in hemoglobin based biosensor. *Mater. Today. Proc.* **33**, 139 (2020)
 38. Umut, E.: Magnetic Properties of Manganese Ferrite (MnFe₂O₄) Nanoparticles synthesized by Co-precipitation method. *Hittite J. Sci. Eng.* **6**, (4)243 (2019)
 39. Majid Niaz Akhtar: Hafiza Ayesha Siddiqab, Muhammad Shahid Nazirc and Muhammad9Azhar Khand; Preparations and tailoring of structural, magnetic properties of rare earths (REs) doped nanoferrites for microwave high frequency applications. *Ceram. Int.* **46**, 26521 (2020)
 40. Chandunika, R.K., Vijayaraghavan, R., Sahu, N.K.: Magnetic hyperthermia application of MnFe₂O₄ nanostructures processed through solvents with the varying boiling point. *Mater. Res. Exp.* **7**, 064002 (2020)
 41. Rafique, M.Y., Li-Qing, P., Javed, Q., Iqbal, M.Z., Hong-Mei, Q., et al.: Growth of monodisperse nanospheres of MnFe₂O₄ with enhanced magnetic and optical properties. *Chin. Phys. B* **22**, 107101–107107 (2013)
 42. Gnanaprakash, G., Philip, J., Raj, B.: Effect of divalent metal hydroxide solubility product on the size of ferrite nanoparticles. *Mater. Lett.* **61**, 4545–4548 (2007)
 43. Jauhar, S., Singhal, S., Dhiman, M.: Manganese substituted cobalt ferrites as efficient catalysts for H₂O₂ assisted degradation of cationic and anionic dyes: their synthesis and characterization. *Appl. Catal. A* **486**, 210 (2014)

Publisher's Note Springer Nature remains neutral with regard to jurisdictional claims in published maps and institutional affiliations.

Springer Nature or its licensor (e.g. a society or other partner) holds exclusive rights to this article under a publishing agreement with the author(s) or other rightsholder(s); author self-archiving of the accepted manuscript version of this article is solely governed by the terms of such publishing agreement and applicable law.